Toward an Image-Guided Microbeam Radiation Therapy Using Gadolinium-Based Nanoparticles

Géraldine Le Duc,[†] Imen Miladi,[‡] Christophe Alric,[‡] Pierre Mowat,[‡] Elke Bräuer-Krisch,[†] Audrey Bouchet,[†] Enam Khalil,[§] Claire Billotey,[‡] Marc Janier,[‡] François Lux,[‡] Thierry Epicier,[⊥] Pascal Perriat,[⊥] Stéphane Roux,[‡,∥,*] and Olivier Tillement[‡]

[†]ID17 Biomedical Beamline, European Synchrotron Radiation Facility, 6 Rue Jules Horowitz, 38000 Grenoble, France, [‡]Laboratoire de Physico-Chimie des Matériaux Luminescents, UMR 5620 CNRS—UCBL, Université de Lyon, 22 Avenue Gaston Berger, 69622 Villeurbanne Cedex, France, [§]Faculty of Pharmacy, University of Jordan, Amman, Jordan, [⊥]Matériaux Ingénierie et Science, UMR 5510 CNRS—INSA de Lyon, 7 Avenue Jean Capelle, 69621 Villeurbanne Cedex, France, and [∥]Institut UTINAM, UMR 6213 CNRS—UFC, Université de Franche-Comté, 16 Route de Gray, 25030 Besançon Cedex, France

ABSTRACT Ultrasmall gadolinium-based nanoparticles (GBNs) induce both a positive contrast for magnetic resonance imaging and a radiosentizing effect. The exploitation of these characteristics leads to a greater increase in lifespan of rats bearing brain tumors since the radiosensitizing effect of GBNs can be activated by X-ray microbeams when the gadolinium content is, at the same time, sufficiently high in the tumor and low in the surrounding healthy tissue. GBNs exhibit therefore an interesting potential for image-guided radiotherapy.

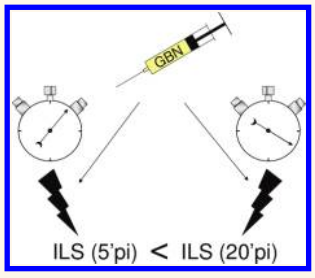

KEYWORDS: nanoparticles · gadolinium · radiosensitizer · medical imaging · theranostic agents

Besides surgery and chemotherapy, radiotherapy constitutes a major modality of cancer therapy. This technique consists in the deposition of a cytotoxic dose in a tumor by irradiation from an external X-ray source. Radiotherapy can be applied in combination with surgery and/or chemotherapy or alone. Despite the tremendous efforts devoted to the improvements of cancer therapy, some results remain however disappointing. For instance, the survival of patients suffering from brain cancer unfortunately has not increased. The incidence of central nervous system tumors is around 10−20 cases/year per 100 000 inhabitants. Glioblastoma is the most aggressive and the most common brain tumor (around 60% among glioma, glioma being already 70% among malignant brain tumors). The median survival is around 1 year after diagnosis, and only 9.8% of patients survive beyond 5 years.[1] Although radiotherapy is presently the most efficient treatment against brain tumors, it suffers from a lack of selectivity in the killing effect, leading to numerous adverse effects in normal tissues surrounding the lesion.[2,3] A better selectivity can however be achieved by microbeam radiation therapy (MRT), as demonstrated by the studies performed at ESRF.[4] What distinguishes MRT from conventional radiotherapy (broad beam) is that normal tissue is more preserved despite the delivery of high doses.[5,6] MRT uses arrays of narrow (∼25−100 μm) microplanar beams (peaks) separated by wider (100−400 μm center-to-center) microplanar spaces (valleys). The height of these microbeams varies from 1 to 100 mm. This geometry implies that the microbeam array dose profile displays a succession of peaks (high dose) and valleys (low dose). The ratio between the central peak and valley doses (PVDR) is an important element for the therapeutic effect of MRT. The normal-tissue toxicity of the irradiation decreases when PVDR increases. High damage of malignant tumors indeed occurs for peak entrance doses of several hundred grays (at least 1 order of magnitude higher than for conventional radiotherapy), whereas normal tissues are surprisingly preserved.[5,6] The application of MRT to the treatment of rats bearing intracerebral 9 L gliosarcoma (9LGS) led for the same sparing of normal tissue to a higher tumor control than broad beam irradiation. As a result, the median survival time increased (MeST) from 19 to 21 days (sham-irradiated control rats) to 40 and 47 days using cross fired, intersecting arrays (10 mm × 10 mm) of 25 μm wide microbeams, spaced 200 μm center-to-center, and skin entrance doses of 625 Gy.[7] MRT offers therefore a great potential for brain cancer therapy

* Address correspondence to stephane.roux@univ-fcomte.fr.

Received for review July 24, 2011 and accepted October 31, 2011.

Published online October 31, 2011
10.1021/nn202797h

since inhibition of the growth of the tumor does not induce alteration of healthy surrounding tissue. Although previous studies provided encouraging results, further improvements are still required for increasing the median survival time. In addition to the modulation of irradiation parameters and/or geometry and the use of chemotherapy, the dose enhancement in the tumor by heavy elements (high Z-elements), which are characterized by a high X-ray photon capture cross-section, constitutes an attractive strategy. Provided that the biodistribution of high Z-elements is well-controlled, it indeed makes possible the deposition of a higher uniform dose in the volume of tumor and a lower dose in normal tissue.[2−4,8] This will be accompanied by a larger production of harmful photoelectrons and radical species. The higher energy absorption and the larger production of reactive species should contribute to a more efficient destruction of the tumor with, at the same time, a better preservation of healthy tissues.

Although many chemicals containing high Z-elements (*e.g.*, iodinated molecules initially conceived as contrast agents for X-ray imaging) have been developed and employed, the results were not satisfying because the amount of radiosensitizers in the tumors is too insufficient and tumor-to-normal tissue high Z-element ratio remains too low.[9] Because of their reduced dimensions, molecules are indeed characterized by a too rapid clearance and by an extravasation from normal blood vessels, which impedes a preferential accumulation in solid tumors, which is essentially based on an enhanced permeability and retention (EPR) effect.[10−15] The intense research activity devoted to nanomedicine that exploits the progress of nanoscience and nanotechnology for medical applications showed that multifunctional nanoparticles exhibit numerous assets for advantageously replacing molecular drugs.[16−20] On the basis of a physical and chemical point of view, the multifunctional particles appear very well suited for achieving image-guided therapy for at least three reasons.[21−29] The first one lies in their size, which can be sufficiently large for avoiding their extravasation from normal vessels and sufficiently small for loading the tumor by passive accumulation (EPR effect) since solid tumors are irrigated by porous vessels.[10−15] The leakage from these abnormal vessels is easily observed for nanoparticles, whose size ranges between 1 and 100 nm. The second reason rests on the possibility to gather, despite the small volume of the nanoparticles, a large range of properties that can be accurately tuned by a convenient choice of components. Nanoparticles can therefore be designed for combining several medical imaging techniques (magnetic resonance imaging (MRI), computed tomography (CT), nuclear medicine imaging (single-photon emission computed tomography (SPECT), positron emission tomography (PET), and/or near-infrared fluorescence (NIRF))[21−23] or for associating imaging and therapeutic activity.[24−29] The latter can be realized either by drug delivery[24,28] or by an interaction between harmless nanoparticles and external physical stimuli.[29] Finally the behavior of the particles (for instance, colloidal stability in biological fluids, biodistribution, and clearance) can be adapted by the control of their size but also by a post-functionalization of the nanoparticles. Choi *et al.* demonstrated that quantum dots (QDs) are renally cleared when their hydrodynamic diameter does not exceed 5−6 nm.[30,31] However renal clearance was also observed for larger nanoparticles (8−10 nm) possessing a different surface chemical composition.[32] Multifunctional nanoparticles containing high Z-elements should therefore appear as an attractive alternative to molecular radiosensitizers. Although many papers are devoted to the capacity of gold and platinum nanoparticles to enhance the dose effects of X-ray beams, no study has been yet performed on gadolinium-based nanoparticles (GBNs).[33−35] Despite a smaller value, the atomic number of gadolinium ($Z = 64$) is sufficiently high for inducing a dose enhancement of X-rays.[36−38] Moreover GBNs are attractive because they can be easily followed up by MRI.[39,40] The possibility to monitor the biodistribution by MRI is indeed crucial for optimizing the effect of radiotherapy since the irradiation can be triggered only when the gadolinium content deduced from MR images is both high in the tumor and low in the surrounding healthy tissue. In order to exploit the attractive features of Gd element and of multifunctional nanoparticles, we developed in this study GBNs for image-guided microbeam radiation therapy and evaluated their potential in the case of the gliosarcoma mouse model (9 L gliosarcoma, 9LGS).

RESULTS AND DISCUSSION

The potential of hybrid nanoparticles composed of a gadolinium oxide core and a fluorescent and hydrophilic polysiloxane shell for medical imaging (MRI, fluorescence imaging) and neutron capture therapy was previously revealed.[41] In order to limit the presence of inactive matter for radio-enhancement, the thickness of the polysiloxane shell was reduced by decreasing the amount of polysiloxane precursors (tetraethyl orthosilicate (TEOS), aminopropyltriethoxysilane (APTES)). In contrast to previous studies, the molar Si to Gd ratio was fixed to 4 instead of over 10.[32,39,41,42] Initially the encapsulation of each gadolinium oxide core aims at both conferring additional characteristics (fluorescence, high colloidal stability) and ensuring the preservation of the core.[43] In order to anticipate a less efficient protective effect of the polysiloxane shell owing to the reduction of its thickness, DTPA derivatives were grafted onto the polysiloxane shell for capturing gadolinium ions, which could be eventually released. DTPA is indeed well known for its ability to form gadolinium chelates, which are widely used as contrast agents for clinical

diagnosis in MRI.[44] Elemental analysis performed by ICP-MS after a thorough purification of the nanoparticles revealed that the encapsulation of the oxide core and the postfunctionalization of the shell by DTPA were carried out with relatively high yields since Si to Gd and DTPA to Gd molar ratios are close to the initial ratios (3.5 *vs* 4 and 0.87 *vs* 1.2, respectively). The reduction of the amount of polysiloxane shell precursors led, as expected, to a decrease of the hydrodynamic diameter (D_h = 2 nm, while D_h > 8 nm when Si/Gd > 10) (Figure 1a). Despite the difficulty in observing these ultrasmall nanoparticles, HR-TEM experiments confirmed that the diameter of gadolinium oxide nanoparticles embedded in a polysiloxane shell does not exceed 2 nm (Figure 2a and b). The cores have a size distribution with an average size of 1.1 nm and a mean standard deviation of 0.6 nm (Figure 2a). Although the contrast of particles is blurred by that of the supporting carbon film, a gray halo is visible around Gd_2O_3 cores due to the presence of the polysiloxane shell (Figure 2b).

The presence of polysiloxane is confirmed by nanoprobe EELS spectra comparing the Si-$L_{2,3}$—Gd-$N_{4,5}$ ionization edges from GBN before and after synthesis of the polysiloxane network (Figure 2c). After usual background subtraction, the spectrum of the nanoparticles after hydrolysis condensation of polysiloxane precursors exhibits a Si-$L_{2,3}$ edge with a shape similar to that of a SiO_2 reference (Figure 2d). However the visualization of the core shell structure is very difficult to observe and requires calculation from TEM phase-contrast imaging at low spatial resolution (Figure 2e).

Arrows in Figure 2e point out isolated particles where the dense Gd_2O_3 core appears darker than the lighter surrounding polysiloxane shell. Projected potential calculations based on the atomic structure of crystalline, cubic Gd_2O_3 and vitreous silica provide an image of a core (diameter: 1 nm) embedded in a polysiloxane shell (thickness: 0.5 nm) (Figure 2e, upper part of the inset). This result is in accordance with the diameter obtained by photon correlation spectroscopy (PCS). For comparison the lower part of the inset of Figure 2e displays the projected potential calculations applied to TEM phase-contrast imaging at low spatial resolution of gadolinium oxide cores before encapsulation.

The grafting of DTPA confers to the nanoparticles a high colloidal stability at pH 7.4, although the zeta potential is close to 0 mV (3.0 mV). It must be pointed out that the colloidal stability is preserved in aqueous solution containing a high concentration of sodium chloride since no large agglomerate was detected by PCS. After NaCl addition to a GBN colloid, the hydrodynamic diameter, which was equal to 2 nm in water, increased to 4.2 nm (Figure 1b). These results indicate that the high colloidal stability of the aqueous GBN solution is ensured by a process that does not rest on the electrostatic repulsion; otherwise, precipitation would be observed in saline solution.

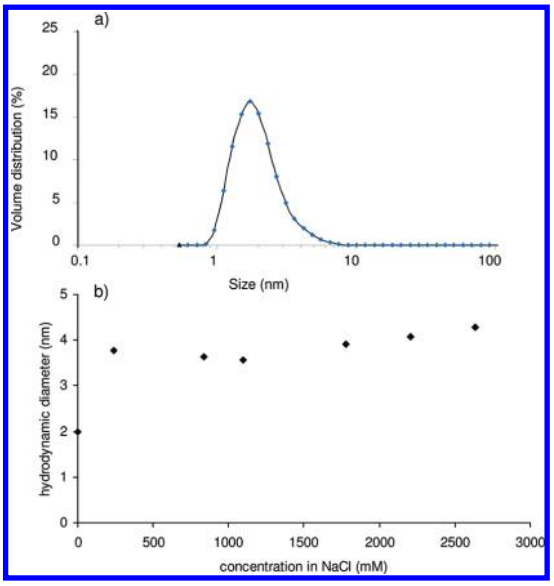

Figure 1. (a) Size distribution of GBN after functionalization determined by photon correlation spectroscopy. (b) Hydrodynamic diameter of GBNs in aqueous solution containing NaCl.

The *in vitro* MRI and synchrotron radiation computed tomography (SRCT) experiments showed that the presence of GBNs in aqueous solutions induces an enhancement of the contrast, which increases with the gadolinium concentration (Figure 3).

The ability of GBNs to behave as efficient positive contrast agents for MRI was assigned both to the high longitudinal relaxivity r_1 (r_1 = 9.4 s^{-1} mM^{-1} at 60 MHz) and to the value of the transverse to longitudinal relaxivities ratio (r_2/r_1 = 1.13). These features can be exploited for monitoring the behavior of GBNs in 9LGS-bearing rats after an intravenous injection of an aqueous GBN colloid ([Gd^{3+}] = 40 mM, V = 1.4 mL).

MRI clearly shows that the nanoparticles are present in the tumor since a strong positive contrast appears in the right hemisphere of the brain a few minutes after the injection. The delineation of the tumor is clearly visible and can be observed for 45 min at least (Figure 4).

This visual observation is corroborated by the intensity variation of the MR signal in the right hemisphere (*i.e.*, the hemisphere containing the tumor) compared to that in the left hemisphere. In other words, the contrast enhancement (EHC), which reflects the gadolinium content in the imaged tissue, is higher in the right hemisphere (RH) than in the left one (LH) after intravenous injection of GBN (EHC(RH)/EHC(LH) > 1, Table 1). Moreover this ratio significantly increases by a factor of 1.68 when the delay between the image acquisition and the injection varies from 5 to 20 min ($[(EHC(RH)/EHC(LH)]_{20}/[(EHC(RH)/EHC(LH)]_5$ = 1.68, Table 1). As expected, the differences are more pronounced when the comparison is performed between the contrast enhancement of smaller regions of interest located in tumor (GS) and in normal tissue (NT) (Figure 5 and Table 1).

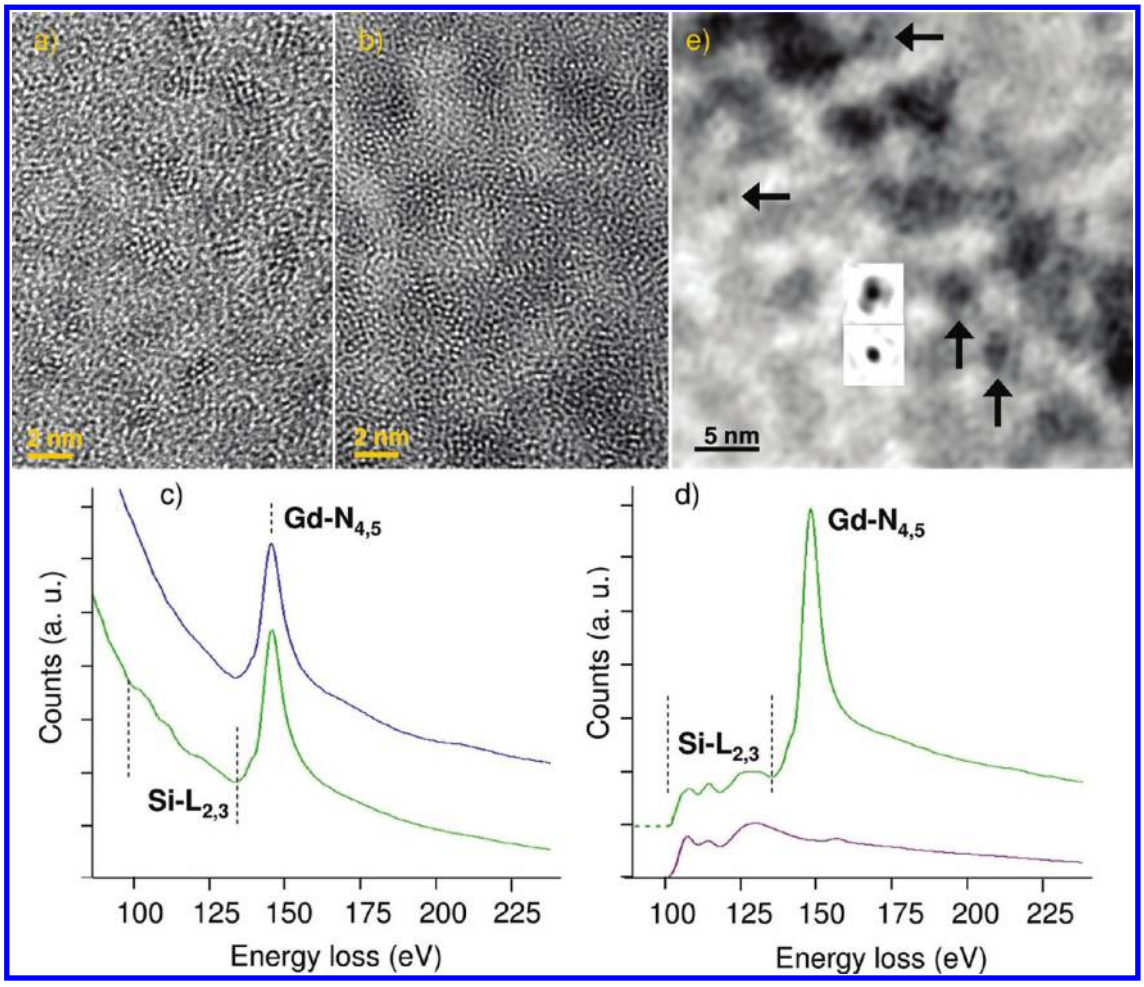

Figure 2. HR-TEM of gadolinium oxide nanoparticles (a) before and (b) after encapsulation in a polysiloxane shell. (c) Nanoprobe EELS spectra of gadolinium oxide cores before (blue curve) and after (green curve) encapsulation in a polysiloxane shell. (d) Comparison of EELS spectra (after background subtraction) of polysiloxane-coated gadolinium oxide nanoparticles (green curve) and silica (purple curve). (e) TEM phase-contrast imaging at low spatial resolution of gadolinium oxide cores after encapsulation in a polysiloxane shell (insets show projected potential calculations of gadolinium oxide after and before polysiloxane formation (top and bottom, respectively)).

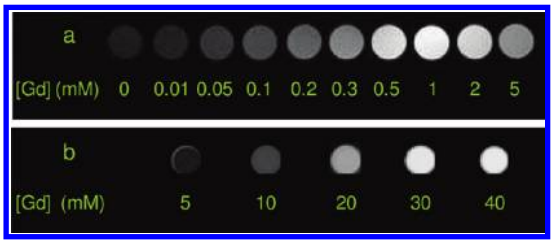

Figure 3. T_1-weighted (a) and SRCT (b) images of phantoms containing various GBN concentrations.

Figure 5 depicts the temporal evolution of the MRI signal. It clearly shows that the gadolinium content in the normal tissue (left hemisphere) increases until 5 min and decreases afterward, while the content in the tumor reaches a plateau. Consequently these results suggest that the amount of nanoparticles is more and more important in the right hemisphere (and peculiarly in the tumor) than in the left hemisphere, between 5 and 30 min after injection. To determine the particle distribution in the brain, *ex vivo* elemental analyses by ICP-MS were performed separately on the right and left hemispheres for different delays between injection and euthanasia (Figure 6). The amount of gadolinium in the right hemisphere (*i.e.*, containing the tumor) is larger than in the left hemisphere even 5 min after the intravenous injection (Figure 6 and Table 1). The difference in gadolinium content between the hemispheres is assigned to the presence of a denser vasculature around the tumor and a disrupted blood brain barrier, which are responsible for a greater blood volume and an enhanced permeability and retention effect, respectively.[10−15,18,19]

Figure 6 shows the decrease of the gadolinium concentration when the delay between injection and euthanasia increases. This decrease is more striking in the left hemisphere, as confirmed by the increase of the ratio of gadolinium content in the right and left hemispheres between 5 and 20 min after the intravenous injection of GBN ($[\tau_{Gd}(RH)/\tau_{Gd}(LH)]_{20}/[\tau_{Gd}(RH)/\tau_{Gd}(LH)]_5$ = 1.74, Table 1). It must be pointed out that the value of this ratio, which is determined by ICP, is, as expected,

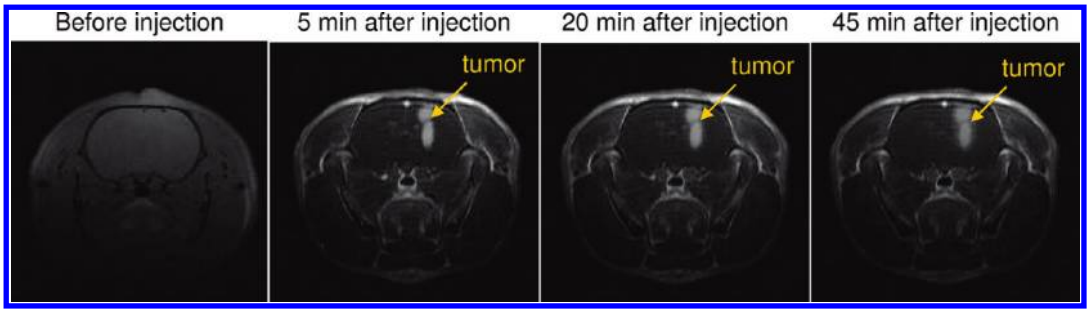

Figure 4. T_1-weighted images of the brain of a 9LGS-bearing rat before and 5, 20, and 45 min after intravenous injection of GBNs.

TABLE 1. Comparison of the Contrast Enhancement (deduced from MR images) and Gadolinium Content (measured by ICP-MS) in Various Regions of the Brain, 5 and 20 Minutes after Intravenous Injection of GBN

delay between the image acquisition and the injection	EHC(RH)/ EHC(LH)[a] (MRI)	τ_{Gd}(RH)/τ_{Gd}(LH)[b] (ICP-MS)	EHC(GS)/ EHC(NT)[c] (MRI)
5 min (A)	7.23	1.17	16.12
20 min (B)	12.15	2.04	60.40
B/A[d]	1.68	1.74	3.75

[a] EHC = contrast enhancement, RH = right hemisphere; LH = left hemisphere. [b] τ_{Gd}(RH) = gadolinium content in the right hemisphere; τ_{Gd}(LH) = gadolinium content in the left hemisphere. [c] GS = gliosarcoma (brain tumor located in the right hemisphere); NT = normal tissue (in the left hemisphere). [d] B/A = $[EHC(RH)/EHC(LH)]_{20}/[EHC(RH)/EHC(LH)]_5$, $[\tau_{Gd}(RH)/\tau_{Gd}(LH)]_{20}/[\tau_{Gd}(RH)/\tau_{Gd}(LH)]_5$, or $[EHC(GS)/EHC(NT)]_{20}/[EHC(GS)/EHC(NT)]_5$.

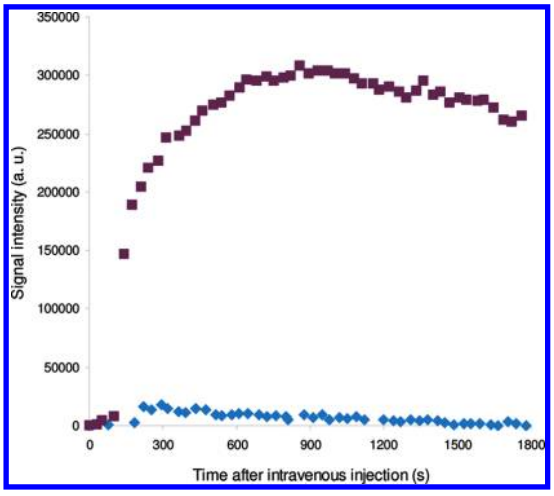

Figure 5. Temporal evolution of the MRI signal in tumor (purple squares) and in an equivalent surface in normal tissue in the left hemisphere (blue diamonds).

very similar to that determined from MR images ($[EHC(RH)/EHC(LH)]_{20}/[EHC(RH)/EHC(LH)]_5$ = 1.68, Table 1). This similarity indicates that MRI is very well suited for guiding radiotherapy since a rapid, precise, and reliable localization of GBN can be established by this noninvasive medical imaging technique. The decrease in the left hemisphere reflects the removal of the nanoparticles from the blood system. The clearance seems to be

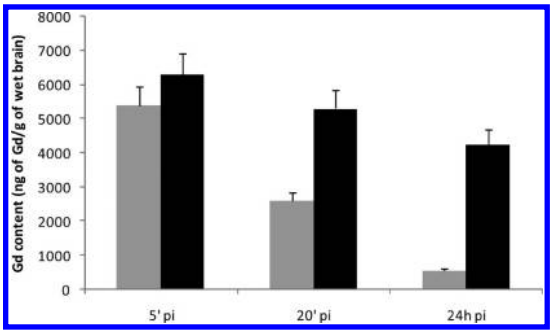

Figure 6. Post-mortem ICP-MS analyses of right (black) and left (light gray) hemispheres of 9LGS-bearing rats that were euthanized 5 min (5′ pi), 20 min (20′ pi), and 24 h (24 h pi) after the intravenous injection of GBN. The tumor was implanted in the right hemisphere.

performed *via* renal excretion since the presence of GBN is attested only in the kidneys, bladder, and urine by the techniques (MRI and SRCT) permitted by the imaging multimodality of the GBN (Figure 7).

The ICP-MS analysis of the urine indicates that up to 30% of gadolinium can be removed by urine during the first hour after intravenous injection. The renal clearance of GBN, which is favored by their small hydrodynamic diameter, leads to the elimination of particles in excess and should avoid any long-term toxicity.[30−32] The slower decrease of the gadolinium content in the right hemisphere confirms that a significant part of the nanoparticles are trapped in the tumor, this accumulation being probably driven by the EPR effect. The accumulation of GBN in the tumor volume attested by MRI and ICP appears favorable for radiotherapy.

For evaluating the dose enhancement effect of the GBN, 9LGS-bearing rats were exposed to MRT 5 and 20 min after intravenous injection. The survival of these rats was compared to the survival of untreated rats and of MRT-only treated rats. The irradiated-only animals had a median survival time (MeST) of 47 days, which corresponds to an increase in lifespan (ILS) of 147% when compared to untreated controls of the present study (MeST for untreated rats = 19 days) (Figure 8).

The MeST was extended to 90 days by performing MRT 20 min after intravenous injection of GBNs (ILS = 373%), while it was shortened to 34 days by reducing

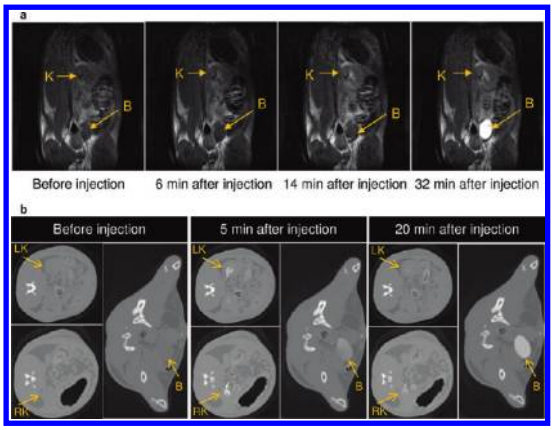

Figure 7. (a) T_1-weighted images of a slice including a kidney (K) and the bladder (B) of a rat before and 6, 14, and 32 min after intravenous injection of GBN. (b) SRCT images of a series of successive transverse slices including the right and left kidneys (RK and LK, respectively) and the bladder (B) of a 9LGS-bearing rat. The images were recorded before and 5 and 20 min after the intravenous injection of GBN.

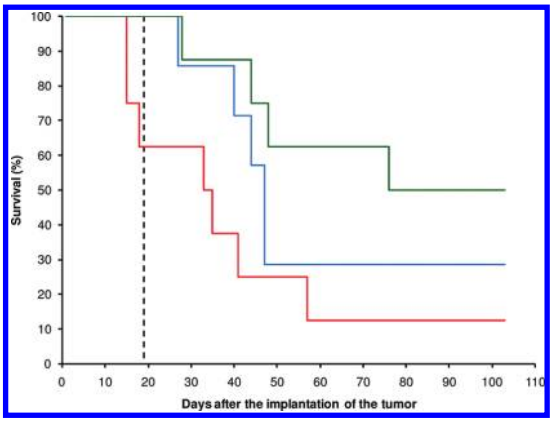

Figure 8. Survival curve comparison obtained on 9LGS-bearing rats without treatment (black dashed curve, $n = 4$ rats), only treated by MRT (blue curve, $n = 7$), and treated by MRT 5 min (red curve, $n = 8$) and 20 min (green curve, $n = 8$) after GBN intravenous injection during 103 days after tumor implantation. The MRT irradiation was done in cross-fired mode, using 50 μm wide microbeams, with a spacing of 211 μm between the beams. The skin entrance dose was set at 400 Gy for the peak and 20 Gy for the valley.

the delay between nanoparticle injection and MRT to 5 min (ILS = 78%). Remarkably, 4 rats in 8 were still alive 100 days after the tumor implantation in the group of animals that were irradiated 20 min after injection of GBNs. The lifespan of these survivors has been multiplied by a factor 5 (ILS = 373%). This experiment obviously evidences a high radiosensitizing effect of gadolinium-based nanoparticles. The efficiency of MRT can be therefore improved by a GBN delivery by intravenous injection prior to the irradiation. However it appears that the delay between the administration of the nanoparticles and the irradiation is a key parameter since a beneficial effect on the survival is observed when the MRT is performed 20 min after injection, while the irradiation performed 5 min after injection is, on the contrary, detrimental for the survival (Figure 8). The MeST shortening observed when MRT was performed 5 min after the intravenous injection is not due to an intrinsic toxic effect of the nanoparticles or of the X-ray microbeams since the lifespan of the rats treated only by MRT or by MRT 20 min after intravenous injection increased. The difference observed between these three treatments has then to be interpreted on the basis of the radiosensitizing effect of GBNs only. In this context, the contrasted observations are certainly related to the difference in the distribution of GBNs within the brain, as highlighted by MRI and ICP-MS experiments. Precisely, even if the amount in the right hemisphere (tumor bearing) is slightly lower 20 min than 5 min after the intravenous injection, the survival of rats irradiated 20 min after injection is longer. This is due to a greater difference in the gadolinium content between the hemispheres that results from a greater particle elimination in the same left hemisphere (Figure 6). Therefore, although the amount of nanoparticles in the tumor is an important parameter, the amount of nanoparticles in healthy tissue is probably still more crucial because healthy tissue can be seriously altered by the dose enhancement of X-rays induced by the presence of particles. This clearly indicates the benefit that can be derived from the monitoring of therapeutic agents by medical imaging.

CONCLUSION

In conclusion, the combination of GBNs and MRT improves the survival of rats bearing aggressive brain tumors. The efficacy of this binary therapeutic system mainly rests on the difference of gadolinium content between tumor and healthy tissue. Since the latter depends on the delay between irradiation and injection, the possibility to follow up GBNs by MRI constitutes an interesting asset for determining the most suitable moment for irradiation. Gadolinium-based nanoparticles obviously exhibit the properties required for the theranostic agents: contrast enhancement of medical imaging (MRI, CT), therapeutic activity (dose enhancement of X-ray microbeams), and a safe behavior after intravenous injection (passive accumulation in the tumor, renal clearance). Their use for image-guided radiotherapy, the first step toward personalized therapy, can be therefore envisaged.

MATERIALS AND METHODS

Chemicals. Gadolinium chloride hexahydrate (99%, Nano-H, France), sodium hydroxide (99%, Sigma Aldrich), diethylene glycol (>99%, SDS), tetraethyl orthosilicate ($Si(OC_2H_5)_4$, TEOS, 98%, Aldrich), (3-aminopropyl)triethoxysilane ($H_2N(CH_2)_3$-$Si(OC_2H_5)_3$, APTES, 99%, Aldrich), diethylenetriaminepentaacetic dianhydride (DTPADA, 98%, Aldrich), triethylamine (TEA, 99%, Aldrich), anhydrous dimethylsulfoxyde (DMSO, Aldrich), and

anhydrous *N*,*N*-dimethylformamide (DMF, Sigma) were used for the synthesis and the functionalization of GBN.

Preparation of Gadolinium Oxide Cores. Gadolinium chloride salt (5.576 g, $GdCl_3 \cdot 6H_2O$) was placed in 100 mL of diethylene glycol (DEG) at room temperature under vigorous stirring. The suspension was heated at 140 °C until the total dissolution of gadolinium chloride salt (about 1 h). When the solution was clear, sodium hydroxide solution (4 mL, 3.38 M) was added dropwise under vigorous stirring. Afterward, the solution was heated and stirred at 180 °C for 3 h. A transparent colloid of gadolinium oxide nanoparticles was obtained and can be stored at room temperature for weeks without alteration.

Coating of Gadolinium Oxide Cores by a Polysiloxane Shell. The silane precursors (APTES (10.1 mL) and TEOS (6.4 mL)) and hydrolysis solution (aqueous Et_3N in DEG (0.1 M of TEA, 10 M of water)) were sequentially and alternatively added to a 400 mL DEG solution containing Gd_2O_3 nanoparticles ([Gd] = 45 mM) under stirring at 40 °C. The Si to Gd molar ratio is fixed to 4, and the proportion of the polysiloxane shell precursors is 60% APTES/40% TEOS. The whole addition of silane precursors and hydrolysis solution is performed in six steps. Each step consists in the addition to the colloid of a portion of the silane precursors mixture (for the first step, 5%; for the second step, 15%; and for the other ones, 20%) followed by the addition of the hydrolysis solution mixture (for the first step, 5%; for the second step, 15%; and for the other ones, 20%). The delay between both additions is one hour. After the last addition, the final mixture was stirred for 48 h at 40 °C.

Functionalization of the Polysiloxane Shell by DTPADA. To stabilize the particles in a biological environment and to capture released Gd^{3+} ions, nanoparticles were functionalized by highly hydrophilic and chelating molecules, DTPADA. The grafting of DTPADA onto the polysiloxane shell of the nanoparticles is rendered possible by the presence of amine groups since APTES was used for the synthesis of the shell. A 100 mL amount of crude GBN colloid (*vide supra*) was mixed with anhydrous DMSO (20 mL) containing DTPADA (DTPADA/APTES molar ratio 1.1, *i.e.*, 4.25 g of DTPADA) and stirred for 1 h.

Purification of GBNs. To transfer nanoparticles from DEG to water, nanoparticles were precipitated in 500 mL of acetone. After centrifugation, the supernatant was removed. The white powder was washed with an ethanol/acetone mixture (v/v 85/15) by three cycles of dispersion−centrifugation (10 min at 3500 rpm). The supernatant was removed after each centrifugation. Then the white powder was dispersed in water. The purification of nanoparticles was performed by tangential centrifugation in Vivaspin (5 kDa). A typical procedure consists in centrifugation of 20 mL of aqueous colloid until the volume was 10 mL. Afterward the GBN aqueous suspension, which is retained by the membrane, was diluted by the addition of deionized water (10 mL), while the filtrate containing the impurities was removed. The cycle "tangential centrifugation−dilution" was repeated 10 times.

Size Measurement and Structural Characterization. Direct measurement of the size distribution of the nanoparticles was performed with the size analyzer NanoS PCS from Malvern Instruments. Measurements were directly taken on the colloid after surface modification of the nanoparticles.

Confirmation of sizes was obtained from high-resolution transmission electron microscopy (HRTEM) performed at CLYM (Centre Lyonnais de Microscopie) with a JEOL 2010F microscope equipped with a Gatan Digi-PEELS energy filter in order to analyze the Si-$L_{2,3}$ and Gd-$N_{4,5}$ ionization edges with electron energy-loss spectroscopy (EELS). Drops of colloidal solutions were deposited on dedicated TEM carbon grids and observed after natural drying.

Inductively Coupled Plasma Mass Spectrometry (ICP-MS) Analysis. Determination of gadolinium content in colloids, in the right and left hemispheres of the brain and in urine, was performed by ICP-MS analysis (Agilent 7500ce). Before measuring Gd concentration, samples of colloidal solution were diluted in 0.5 M HNO_3 (1:2500, v/v) and in HNO_3 (2%, 2 ppb In; 1:50, v/v). The determination of gadolinium content in right and left hemispheres of the brain and in urine required their dissolution in *aqua regia*. The resulting solutions were diluted in HNO_3 (2%, 2 ppb In, 1:300 v/v for brain and 1:3000 v/v for urine).

Imaging and MRT Experiments. All operative procedures related to animal care strictly conformed to the Guidelines of the French Government with licenses 380325 and A3818510002. All experiments were performed under anesthesia with the following parameters: 5% isoflurane for induction and intraperitoneal injection of xylazine/ketamine (64.5/5.4 mg kg^{-1}) for maintenance.

Brain Tumor Inoculation. The 9 L gliosarcoma (9LGS) cells were implanted in the brain of male Fisher 344 rats (Charles River, France). Anesthetized animals were placed on a stereotactic frame, and 10^4 9LGS cells suspended in 1 μL of culture medium with antibiotics were injected through a burr hole in the right caudate nucleus (3.5 mm lateral to the bregma, 6 mm below the skull surface).

Preparation of Injectable Solution. After tangential filtration, a concentrated colloid (GBNs in water, [Gd] = 100 mM) was diluted by aqueous solution containing NaCl and HEPES in order to obtain an intravenous use solution ([Gd] = 40 mM, [NaCl] = 145 mM, [HEPES] = 10 mM). pH was adjusted to 7.4. Before use, this solution was filtered onto a syringe filter with a nylon membrane (pore diameter 0.22 μm).

Drug Injection. The aqueous GBN ($[Gd^{3+}]$ = 40 mM, [NaCl] = 145 mM, [HEPES] = 10 mM) colloid was manually injected in the saphena vein at a 1.4 mL volume using a 2 mL syringe and a 26 G needle.

MR Imaging. Images were acquired before and after injection using a 7 T Bruker imaging system (Biospec; Brüker, Erlangen, Germany) equipped with a 400 mT/m gradient. Anaesthesia was induced with 3−4% isoflurane and maintained with 1.5−2% isoflurane in a mixture of O_2/N_2 (25%/75%).

The imaging protocol consisted of a T_2-weighted TurboRARE SE sequence (TE = 36 ms, TR = 4200 ms, field of view = 2.56 cm, matrix = 256 × 256, slice thickness = 0.65 mm), T_1-weighted FLASH images (TE = 3.6 ms, TR = 86.07 ms, field of view = 2.56 cm, matrix = 256 × 256, slice thickness = 0.65 mm), and a dynamic series of transverse slices centered on the rat brain, obtained with a T_1-weighted MSME sequence (TR/TE = 113.4/10.6 ms, slice thickness = 1.5 mm, field of view = 5 cm, matrix = 256 × 256).

The intravenous injection of GBN ([Gd] = 40 mM) was performed during the fourth repetition of the dynamic acquisition. The duration of each repetition was about 60 s.

The measurement method of enhancement after injection of gadolinium on MR imaging was performed as follows. Regions of interest (ROIs) with the same area were drawn, and the signal in this area on each image was measured. Positive enhancement of the signal (EHC) in each area was calculated as $(S_t - S_0)/S_0$, where S_t was the signal intensity value measured at each time after injection, and S_0 the signal value before injection. To compare the positive enhancement of the signal in healthy tissue and tumor, the enhancement of a ROI in the right hemisphere (containing the tumor) is divided by the enhancement of a ROI with an identical area but located in the left hemisphere (normal tissue) for a definite time ($[EHC(RH)/EHC(LH)]_t$, $[EHC(GS)/EHC(NT)]_t$ with t = 5 and 20 minutes, please see Table 1). The ROIs of RH and LH have the same area. They cover the right and the left hemispheres, respectively. The ROIs of GS and NT have the same area, which is smaller than the area of the ROIs of the RH and LH. They cover a small region of the tumor (GS) and of the normal tissue in the left hemisphere (NT), respectively. The temporal evolution of the EHC(RH)/EHC(LH) ratio is obtained by dividing the EHC(RH)/EHC(LH) ratio calculated for the image recorded 20 min after the injection of GBN by the one calculated 5 min after the injection (*i.e.*, $[EHC(RH)/EHC(LH)]_{20}/[EHC(RH)/EHC(LH)]_5$). The temporal evolution of the EHC(GS)/EHC(NT) ratio was obtained in a similar way ($[EHC(GS)/EHC(NT)]_{20}/[EHC(GS)/EHC(NT)]_5$).

SRCT Imaging. SRCT images of phantoms containing GBNs at various gadolinium concentrations and *in vivo* imaging were performed at the biomedical beamline ID17 of the European Synchrotron Radiation Facility (Grenoble, France). The SRCT images were obtained using a monochromatic X-ray beam tuned slightly above the gadolinium K-edge energy (50.239 keV). The acquisition was performed during a rotation of the sample of 360° around a vertical axis by means of a rotation stage. The attenuation was measured with a cryogenically cooled, high-purity germanium detector. The cross-sectional

images obtained by SRCT experiments were calculated from the numerous projections measured at small angular intervals. The data processing was performed under IDL software called SNARK code (University of Pennsylvania, Philadelphia).

In the case of *in vivo* imaging, the rats were anesthetized by means of an intraperitoneal injection of a mixture of xylazine/ketamine before placement in a vertical stereotatic holder screwed on the rotation motor. GBN colloids were injected in the saphena vein. The behavior of nanoparticles was followed up over 1 h.

Radiation Source and MRT Setup. MRT was performed at the ID17 biomedical beamline at the European Synchrotron Radiation Facility (Grenoble, France). MRT uses X-rays emitted tangentially to the ring from relativistic electron bunches circulating in a storage ring. The wiggler source produces a white spectrum of photons that extends after filtration (Be (0.5 mm), C (1.5 mm), Al (1.5 mm), and Cu (1.0 mm)) from 50 to 350 keV (mean energy of 90 keV). The quasi-laminar beam is spatially fractionated into an array of microbeams by using an adjustable multislit collimator positioned 41.7 m from the photon source and 100 cm upstream from the head of the animals. Upstream from the multislit collimator, the dose rate within a homogeneous field of 10 mm $\times$ 10 mm was approximately 90 Gy s^{-1} mA^{-1}. Downstream of the multislit collimator, the peak entrance dose within the microbeam was $\sim$72 Gy s^{-1} mA^{-1}.

***In Vivo* Irradiation Methods.** Ten days after tumor inoculation, the animals were positioned prone on a Kappa-type goniometer (Huber,Germany) in front of the X-ray source, on a homemade Plexiglas frame. Rats were first placed perpendicularly to the beam and received a lateral irradiation, from their anatomically right side to their left. Then, a 90° angle was applied to the motorized goniometer, and the second irradiation was performed in the anatomically anteroposterior direction. The field of irradiation was fixed at 10.5 mm height and 8 mm width and was centered at the theoretical center of the tumor (*i.e.*, 3.5 mm lateral to the bregma, 6 mm deep in the skull in the right hemisphere). The microbeams were 50 μm wide with an on-center distance fixed at 211 μm. The total irradiation procedure lasted about 2 min. Animal immobility during exposure was checked on three control video screens located in the control hutch. A series of 27 rats was divided into untreated rats (n = 4), MRT -treated rats without GBN injection (n = 7), treated rats with a 5 min delay between GBN injection and MRT (n = 8), and treated rats with a 20 min delay between GBN injection and MRT (n = 8). These delays between drug injection and MRT were chosen according to results obtained by MRI. The spatial configuration of the microbeams was checked by radiochromic films (Gafchromic, HD-810).

Survival Analysis. The rats were followed up at the animal facility after the irradiation. At a later tumor stage, rats were euthanized by intracardiac injection of pentobarbital sodium less than 1 day before their anticipated death as judged by clinical signs. Some of them were found dead. The time between implantation and death was recorded as survival time (one day was added for euthanized rats). The median survival time (MeST) postimplantation was calculated, and Kaplan–Meier survival data were plotted *versus* time after tumor implantation. The increase in lifespan in percent (ILS) characterizes the difference between median survival time for treated and untreated rats divided by the median survival time for untreated rats.

Acknowledgment. We wish to thank Maxime Saint-Jean for his valuable help in the large-scale synthesis of GBNs and the ESRF Biomedical Beamline for beamtime and support with a special mention to Thierry Brochard and Dominique Dallery. Thanks are due to the CLYM (http:\\clym.insa-lyon.fr) for the access to the 2010F microscope.

REFERENCES AND NOTES

1. Stupp, R.; Mayer, M.; Kann, R.; Weder, W.; Zouhair, A.; Betticher, D. C.; Roth, A. D.; Stahel, R. A.; Majno, S. B.; Peters, S.; *et al*. Neoadjuvant Chemotherapy and Radiotherapy Followed by Surgery in Selected Patients with Stage IIIB Non-Small-Cell Lung Cancer: A Multicentre Phase II Trial. *Lancet Oncol.* **2009**, *10*, 785–793.
2. McMahon, S. J.; Medenhall, M. H.; Jain, S.; Currell, F. Radiotherapy in the Presence of Contrast Agents: A General Figure of Merit and its Application to Gold Nanoparticles. *Phys. Med. Biol.* **2008**, *53*, 5635–5651.
3. Kobayashi, K.; Usami, N.; Porcel, E.; Lacombe, S.; Le Sech, C. Enhancement of Radiation Effect by Heavy Elements. *Mutat. Res.* **2010**, *704*, 123–131.
4. Bräuer-Krisch, E.; Serduc, R.; Siegbahn, E. A.; Le Duc, G.; Prezado, Y.; Bravin, A.; Blattmann, H.; Laissue, J. A. Effects of Pulsed, Spatially Fractionated, Microscopic Synchrotron X-Ray Beams on Normal and Tumoral Brain Tissue. *Mutat. Res.* **2010**, *704*, 160–166.
5. Laissue, J. A.; Geiser, G.; Spanne, P. O.; Dilmanian, F. A.; Gebbers, J.-O.; Geiser, M.; Wu, X.-Y.; Makar, M. S.; Micca, P. L.; Nawrocky, M. M.; *et al*. Neuropathology of Ablation of Rat Gliosarcomas and Contiguous Brain Tissues Using a Microplanar Beam of Synchrotron-Wiggler-Generated X-Rays. *Int. J. Cancer* **1998**, *78*, 654–660.
6. Dilmanian, F. A.; Button, T. M.; Le Duc, G.; Zhong, N.; Pena, L. A.; Smith, J. A. L.; Martinez, S. R.; Bacarian, T.; Tammam, J.; Ren, B.; *et al*. Response of Rat Intracranial 9L Gliosarcoma to Microbeam Radiation Therapy. *Neuro-oncology* **2002**, *4*, 26–38.
7. Regnard, P.; Le Duc, G.; Bräuer-Krisch, E.; Tropres, I.; Siegbahn, E. A.; Kusak, A.; Clair, C.; Bernard, H.; Dallery, D.; Laissue, J. A.; *et al*. Irradiation of Intracerebral 9L Gliosarcoma by a Single Array of Microplanar X-Ray Beams from a Synchrotron: Balance between Curing and Sparing. *Phys. Med. Biol.* **2008**, *53*, 861–878.
8. Pradhan, A. K.; Nahar, S. N.; Montenegro, M.; Yu, Y.; Zhang, H. L.; Sur, C.; Mrozik, M.; Pitzer, R. M. Resonant X-Ray Enhancement of the Auger Effect in High-Z Atoms, Molecules, and Nanoparticles: Potential Biomedical Applications. *J. Phys. Chem. A* **2009**, *113*, 12356–12363.
9. Rabin, O.; Perez, J. M.; Grimm, J.; Wojtkiewicz, G.; Weissleder, R. An X-Ray Computed Tomography Imaging Agent Based on Long-Circulating Bismuth Sulphide Nanoparticles. *Nat. Mater.* **2006**, *5*, 118–122.
10. Seymour, L. W.; Myamoto, Y.; Maeda, H.; Brereton, M.; Strohalm, J.; Ulbrich, K.; Duncan, R. Influence of Molecular Weight on Passive Tumour Accumulation of a Soluble Macromolecular Drug Carrier. *Eur. J. Cancer* **1995**, *31A*, 766–770.
11. Noguchi, Y.; Wu, J.; Duncan, R.; Strohalm, J.; Ulbrich, K.; Akaike, T.; Maeda, H. Early Phase of Tumor Accumulation of Macromolecules: A Great Difference in Clearance Rate between Tumor and Normal Tissues. *Jpn. J. Cancer Res.* **1998**, *89*, 307–314.
12. Maeda, H.; Sawa, T.; Konno, T. Mechanism of Tumor-Targeted Delivery of Macromolecular Drugs, Including the EPR Effect in Solid Tumor and Clinical Overview of the Prototype Polymeric Drug SMANCS. *J. Controlled Release* **2001**, *74*, 47–61.
13. Bergers, G.; Benjamin, L. E. Angiogenesis: Tumorigenesis and the Angiogenic Switch. *Nat. Rev. Cancer* **2003**, *3*, 401–410.
14. Jang, S. H.; Wientjes, M. G.; Lu, D.; Au, J. L.-S. Drug Delivery and Transport to Solid Tumors. *Pharm. Res.* **2003**, *20*, 1337–1350.
15. Iyer, A. K.; Khaled, G.; Fang, J.; Maeda, H. Exploiting the Enhanced Permeability and Retention Effect for Tumor Targeting. *Drug Discovery Today* **2006**, *11*, 812–818.
16. Ferrari, M. Cancer Nanotechnology: Opportunities and Challenges. *Nat. Rev.* **2005**, *5*, 161–171.
17. Riehmann, K.; Schneider, S. W.; Luger, T. A.; Godin, B.; Ferrari, M.; Fuchs, H. Nanomedicine-Challenge and Perspectives. *Angew. Chem., Int. Ed.* **2009**, *48*, 872–897.
18. Jain, R. K.; Stylianopoulos, T. Delivering Nanomedicine to Solid Tumors. *Nat. Rev. Clin. Oncol.* **2010**, *7*, 653–664.
19. Scheinberg, D. A.; Villa, C. H.; Escorcia, F. E.; McDevitt, M. R. Conscripts of the Infinite Armada: Systemic Cancer Therapy Using Nanomaterials. *Nat. Rev. Clin. Oncol.* **2010**, *7*, 266–276.
20. Minelli, C.; Lowe, S. B.; Stevens, M. M. Engineering Nanocomposites Materials for Cancer Therapy. *Small* **2010**, *6*, 2336–2357.

21. Cai, W.; Chen, X. Nanoplatforms for Targeted Molecular Imaging in Living Subjects. *Small* **2007**, *3*, 1840–1854.
22. Cheon, J.; Lee, J.-H. Synergistically Integrated Nanoparticles as Multimodal Probes for Nanobiotechnology. *Acc. Chem. Res.* **2008**, *41*, 1630–1640.
23. Louie, A. Multimodality Imaging Probes. *Chem. Rev.* **2010**, *110*, 3146–3195.
24. Gianella, A.; Jarzyna, P. A.; Mani, V.; Ramachadran, S.; Calcagno, C.; Tang, J.; Kann, B.; Dijk, W. J. R.; Thijssen, V. L.; Griffioen, A. W.; *et al*. Multifunctional Nanoemulsion Platform for Imaging Guided Therapy Evaluated in Experimental Cancer. *ACS Nano* **2011**, *5*, 4422–4433.
25. Huang, P.; Bao, L.; Zhang, C.; Lin, J.; Luo, T.; Yang, D.; He, M.; Li, Z.; Gao, G.; Gao, B.; *et al*. Folic Acid-Conjugated Silica-Modified Gold Nanorods for X-Ray/CT Imaging-Guided Dual-Mode Radiation and Photo-Thermal Therapy. *Biomaterials* **2011**, *32*, 9796–9809.
26. Peng, C.-L.; Shih, Y.-H.; Lee, P.-C.; Hsieh, T. M.-H.; Luo, T.-Y.; Shieh, M.-J. Multimodal Image-Guided Photothermal Therapy Mediated by 188Re-Labeled Micelles Containing a Cyanine-Type Photosensitizer. *ACS Nano* **2011**, *5*, 5594–5607.
27. Lim, E.-K.; Huh, Y.-M.; Yang, J.; Lee, K.; Suh, J.-S.; Haam, S. pH-Triggered Drug-Releasing Magnetic Nanoparticles for Cancer Therapy Guided by Molecular Imaging by MRI. *Adv. Mater.* **2011**, *23*, 2436–2442.
28. Lammers, T.; Aime, S.; Hennink, W. E.; Storm, G.; Kiessling, F. Theranostic Nanomedicine. *Acc. Chem. Res.* **2011**, *44*, 1029−1038.
29. Bardhan, R.; Lal, S.; Joshi, A.; Halas, N. J. Theranostic Nanoshells: From Probe Design to Imaging and Treatment of Cancer. *Acc. Chem. Res.* **2011**, *44*, 936−946.
30. Choi, H. S.; Liu, W.; Misra, P.; Tanaka, E.; Zimmer, J. P.; Ipe, B. I.; Bawendi, M. G.; Frangioni, J. V. Renal Clearance of Quantum Dots. *Nat. Biotechnol.* **2007**, *25*, 1165–1170.
31. Choi, H. S.; Liu, W.; Liu, F.; Nasr, K.; Misra, P.; Bawendi, M. G.; Frangioni, J. V. Design Considerations for Tumour-Targeted Nanoparticles. *Nat. Nanotechnol.* **2010**, *5*, 42–47.
32. Faure, A.-C.; Dufort, S.; Josserand, V.; Perriat, P.; Coll, J.-L.; Roux, S.; Tillement, O. Control of the *in vivo* Biodistribution of Hybrid Nanoparticles with Different Poly(ethylene glycol) Coatings. *Small* **2009**, *5*, 2565–2575.
33. Hainfeld, J. F.; Dilmanian, F. A.; Slatkin, D. N.; Smilowitz, H. M. Radiotherapy Enhancement with Gold Nanoparticles. *J. Pharm. Pharmacol.* **2008**, *60*, 977–985.
34. Chang, M.-Y.; Shiau, A.-L.; Chen, Y.-H.; Chang, C.-J.; Chen, H. H.-W.; Wu, C.-L. Increased Apoptotic Potential and Dose-Enhancing Effect of Gold Nanoparticles in Combination with Single-Dose Clinical Electron Beams on Tumor-Bearing Mice. *Cancer Sci.* **2008**, *99*, 1479–1484.
35. Porcel, E.; Liehn, S.; Remita, H.; Usami, N.; Kobayashi, K.; Furusawa, Y.; Le Sech, C.; Lacombe, S. Platinum Nanoparticles: A Promising Material for Future Cancer Therapy? *Nanotechnology* **2010**, *21*, 085103
36. Prezado, Y.; Fois, G.; Le Duc, G.; Bravin, A. Gadolinium Dose Enhancement Studies in Microbeam Radiation Therapy. *Med. Phys.* **2009**, *36*, 3568–3574.
37. Pignol, J.-P.; Rakovitch, E.; Beachey, D.; Le Sech, C. Clinical Significance of Atomic Inner Shell Ionization (ISI) and Auger Cascade for Radiosensitization Using IUdr, BUdr, Platinium Salts, or Gadolinium Porphyrin Compounds. *Int. J. Radiat. Oncol. Biol. Phys.* **2003**, *55*, 1082–1091.
38. Regnard, P.; Bräuer-Krisch, E.; Tropres, I.; Keyrilainen, J.; Bravin, A.; Le Duc, G. Enhancement of Survival of 9L Gliosarcoma Bearing Rats Following Intracerebral Delivery of Drugs in Combination with Microbeam Radiation Therapy. *Eur. J. Radiol.* **2008**, *68*, S151–S155.
39. Bridot, J.-L.; Faure, A.-C.; Laurent, S.; Rivière, C.; Billotey, C.; Hiba, B.; Janier, M.; Josserand, V.; Coll, J.-L.; Vander Elst, L.; *et al*. Hybrid Gadolinium Oxide Nanoparticles: Multimodal Contrast Agents for *in vivo* Imaging. *J. Am. Chem. Soc.* **2007**, *129*, 5076–5084.
40. Park, J. Y.; Baek, M. J.; Choi, E. S.; Woo, S.; Kim, J. H.; Kim, T. J.; Jung, J. C.; Chae, K. S.; Chang, Y.; Lee, G. H. Paramagnetic Ultrasmall Gadolinium Oxide Nanoparticles as Advanced T_1 MRI Contrast Agent: Account for Large Longitudinal Relaxivity, Optimal Particle Diameter, and *in vivo* T_1 MR Images. *ACS Nano* **2009**, *3*, 3663–3669.
41. Bridot, J.-L.; Dayde, D.; Rivière, C.; Mandon, C.; Billotey, C.; Lerondel, S.; Sabattier, R.; Cartron, G.; Le Pape, A.; Blondiaux, G.; *et al*. Hybrid Gadolinium Oxide Nanoparticles Combining Imaging and Therapy. *J. Mater. Chem.* **2009**, *19*, 2328–2335.
42. Faure, A.-C.; Hoffmann, C.; Bazzi, R.; Goubard, F.; Pauthe, E.; Marquette, C. A.; Blum, L. J.; Perriat, P.; Roux, S.; Tillement, O. Functionalization of Luminescent Aminated Particles for Facile Bioconjugation. *ACS Nano* **2008**, *2*, 2273–2282.
43. Louis, C.; Bazzi, R.; Marquette, C. A.; Bridot, J.-L.; Roux, S.; Ledoux, G.; Mercier, B.; Blum, L.; Perriat, P.; Tillement, O. Nanosized Hybrid Particles with Double Luminescence for Biological Labeling. *Chem. Mater.* **2005**, *17*, 1673–1682.
44. Caravan, P.; Ellison, J. J.; McMurry, T. J.; Lauffer, R. B. Gadolinium(III) Chelates as MRI Contrast Agents: Structure, Dynamics, and Applications. *Chem. Rev.* **1999**, *99*, 2293–2352.